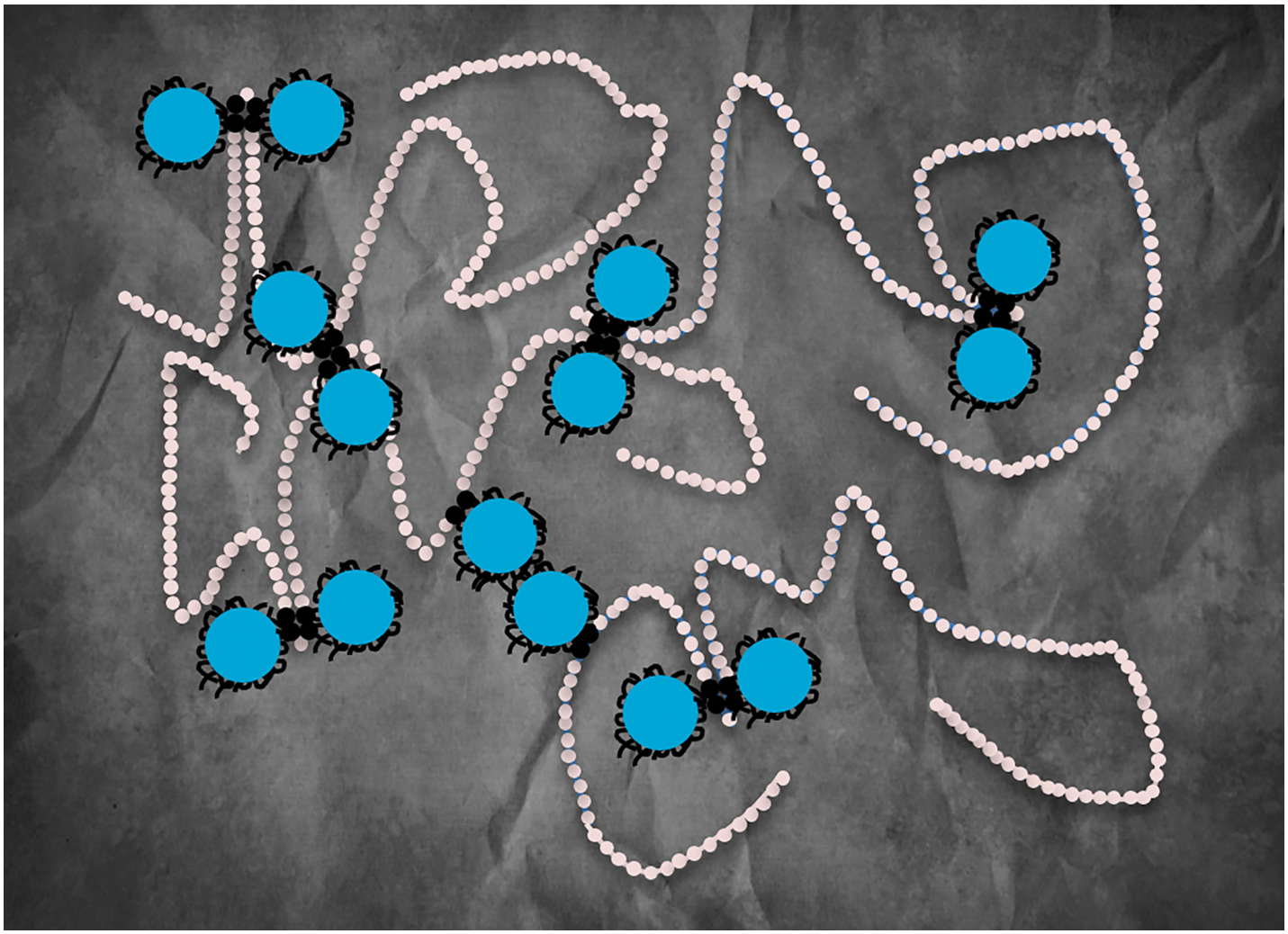

Highlighting research from Delft University of Technology (The Netherlands).

Rheological response of a modified polyacrylamide–silica nanoparticles hybrid at high salinity and temperature

Hybrid of hydrophobically modified polyacrylamide–silica nanoparticles emerged as a promising strategy for achieving enhanced stability and high viscosity. We experimentally explain the role of nanoparticles in bridging between polymer chains leading to an increase in the hydrodynamic radius and consequently the viscosity of the hybrid.

As featured in:

See Mohsen Mirzaie Yegane *et al.*, *Soft Matter*, 2020, **16**, 10198.

ROYAL SOCIETY OF CHEMISTRY

rsc.li/soft-matter-journal

Registered charity number: 207890

Soft Matter

PAPER

View Article Online
View Journal | View Issue

Cite this: *Soft Matter*, 2020, **16**, 10198

Rheological response of a modified polyacrylamide–silica nanoparticles hybrid at high salinity and temperature†

Mohsen Mirzaie Yegane, *[a] Fatemeh Hashemi, [b] Frank Vercauteren, [c] Nicole Meulendijks, [c] Ridha Gharbi, [d] Pouyan E. Boukany [b] and Pacelli Zitha [a]

Received 8th July 2020,
Accepted 30th September 2020

DOI: 10.1039/d0sm01254h

rsc.li/soft-matter-journal

Water-soluble polyacrylamides have often been used to modify flow response in various water-based technologies and industrial processes, including paints, water treatment, paper manufacturing, and chemical enhanced oil recovery. Polymers are susceptible to degradation at combined high salinity and elevated temperature conditions which limits their overall performance. Hybrid mixtures of hydrophobically modified polyacrylamide (HMPAM) with hydrophobically modified silica nanoparticles (NPs) emerged as a promising strategy for achieving enhanced stability and high viscosity in brines having a high total dissolved solids (TDS) content and high hardness at elevated temperatures (>20 wt% TDS, including >1.5 wt% divalent cations at $T > 70$ °C). The rheological response of the hybrids at various concentrations of HMPAM and NPs was examined to investigate the synergic effects. Hybridization of HMPAM with NPs led to a higher viscosity at high salinity and elevated temperature. The viscosity improvement was more pronounced when the concentration of HMPAM was in the semi-dilute regime and concentration of NPs was higher than a critical threshold where the viscosity increased roughly by a factor of 1.5. Here we present the mechanisms of improved viscosity behaviour. The rheological data suggest the role of NPs in the bridging between HMPAM molecules, which in turn increases the hydrodynamic radius and consequently the viscosity of the hybrids.

Introduction

The stability of colloidal systems at high electrolyte concentration is critical for optimum performance of various industrial products and processes, including water-based coatings or paints,[1–3] environmental applications[4–6] and chemical enhanced oil recovery (cEOR).[7–9] In paints, for instance, once the salt concentration in the rust layer at the steel–paint interface exceeds a threshold, premature deterioration of the paint coating is observed.[10]

As a basic cEOR method, polymer injection increases oil recovery over water flooding by viscosifying the aqueous drive water.[11] Partially hydrolysed polyacrylamide (HPAM) is the most commonly utilised polymer for cEOR.[11–14] HPAM is characterized by the presence of negatively charged carboxylic groups along the polymer backbone.[15] Electrostatic repulsion among the carboxylic groups results in the expansion of the coiled HPAM chains, thus increasing the solution viscosity, compared to non-ionic polyacrylamide (PAM).[12] At high ionic strength, however, electrostatic repulsions between the negatively charged groups are almost completely screened by mono- and divalent cations. Therefore, the excluded volume and consequently the molecular size of the polymer chains are reduced.[16] For this reason, HPAM viscosity decreases as salinity increases. At sufficiently high concentrations of divalent cations, complexation of the metal ion by the carboxylate groups occurs leading to polymer precipitation.[17,18] These effects are exacerbated as temperature increases due to further hydrolysis of acrylamide monomers in the polymer backbone.[19]

Several approaches for synthesising water-soluble polymers with improved rheological properties at high salinities up to 20 wt% total dissolved solids (TDS) and temperatures up to 120 °C have been reported.[20–24] Many focus on the substitution

[a] *Department of Geosciences and Engineering, Delft University of Technology, Delft, The Netherlands. E-mail: Mohsen.mirzaieyegane@gmail.com*
[b] *Department of Chemical Engineering, Delft University of Technology, Delft, The Netherlands*
[c] *The Netherlands Organisation for Applied Scientific Research (TNO), High Tech Campus 25, 5656AE Eindhoven, The Netherlands*
[d] *Kuwait Oil Company, Ahmadi, Kuwait*

† Electronic supplementary information (ESI) available: Calculation of the volume fraction of the ligand, pictures of samples to observe the stability of nanoparticles and hybrids over time, details of TEM performed on nanoparticles, tables which include the fitting parameters for Carreau–Yasuda model (eqn (4)), molecular weight estimation of HMPAM and PAM, estimation of overlap concentration, radius of gyration and persistence length for HMPAM and ^{1}H NMR spectrum for *t*-butyl acrylamide. See DOI: 10.1039/d0sm01254h

of the acrylamide monomer by at least another monomer type which can enhance the stability of the polymer at such harsh conditions.[20–22,25] For instance, the incorporation of 2-acrylamido-2-methylpropane sulfonic acid (AMPS)[23,26] and *N*-vinyl-2-pyrrolidone (*N*-VP)[24,26] co-monomers increases tolerance to high salinity particularly to the presence of divalent cations and against thermal hydrolysis respectively. Even though modified polyacrylamides have shown promising results at high temperatures and salinities, they are more expensive than HPAM and need to be overdosed to reach target viscosities since their molecular weight is low.[27] Therefore, the use of such polymers is economically unattractive.

An alternative approach to overcome the above issues consists in combining the polymer with nanoparticles (NPs) to form a hybrid system which is stable at elevated temperature and high salinity. The premise of the new method is that the rheological properties of polymer solution at such harsh conditions can be improved by fine-tuning the polymer–NPs interactions. Several studies demonstrated that hybrid networks can be obtained by the introduction of silica nanoparticles in aqueous media into the macromolecular architecture of associative polymers based on reversible associations.[28–32] Moreover, if the associative polymers also show lower critical solution temperature (LCST) properties, temperature and salting-out may be used to modify the viscoelastic properties of the hybrid network.[28] Kamibayashi *et al.*[33] have shown that associative polymers containing a minor proportion of hydrophobic groups can act as flocculants in aqueous suspension of silica NPs. The flocculation was induced by polymer bridging between silica NPs and led to a significant increase in the viscosity of the suspension. Bhardwaj *et al.*[34] reported improved thermo-resistance and high thermal stability behaviour for nano-size PAM/silica composites. Maghzi *et al.*[35] reported that the viscosity of a PAM/silica hybrid was higher than that of a polyacrylamide solution in the range of tested salinities from 1.4 wt% to 8.4 wt% TDS. Hu *et al.*[36] observed that the addition of silica NPs considerably increases the HPAM viscosity at salinities up to 8 wt% NaCl and temperatures up to 80 °C. Cao *et al.*[37] indicated that the salt-tolerance and heat-resistance properties of a solution containing copolymer of acrylamide and AMPS were improved by the addition of amino-functionalised silica NPs in brines containing up to 8 wt% NaCl and 0.12 wt% $CaCl_2$ at 70 °C. The strong interaction between silica NPs and polymer is chiefly ascribed to hydrogen bonds between the functional groups on polymer molecules including hydroxyl, amide and carboxylate groups and the silanol groups on the surface of NPs.[34,36–38]

The above solutions suffer from several limitations: (a) polymer–NPs hybrids were not investigated for salinities higher than 8.4 wt% which are typical in various industrial processes (b) insufficient information was provided on colloidal stability at high salinity conditions and (c) the role of the polymer concentration, from dilute to semi-dilute regimes, on the rheological response of hybrids was not discussed. To address the limitations of current approaches, we propose a polymer–NPs hybrid system based on the hydrophobic–hydrophobic interaction. This specific interaction enables the development of a system, which is stable and retains sufficiently high viscosity at extreme salinities and elevated temperatures (>20 wt% TDS, including >1.5 wt% divalent cations, and $T > 70$ °C).

In our experiments hydrophobically modified silica NPs were added to a solution of hydrophobically modified polyacrylamide (HMPAM) to facilitate the bridging between polymer chains. Silica NPs were modified by gamma-glycidoxypropyltrimethoxysilane (GPTMS), a low molecular weight organic ligand to provide steric stabilization and ensure the colloidal stability at high salinity.[39] By modification, the surface becomes more hydrophobic than the original bare silica but still has sufficient polarity to allow a good dispersion in water. To describe the colloidal stability of NPs in this work, an extended DLVO (xDLVO)[40–42] theory has been used in different ionic strengths and with or without surface modification of NPs. In order to study the improvement of flow responses of the hybrids, viscosity measurements were performed at various concentrations of HMPAM and NPs.

The results showed that the addition of NPs increases the viscosity of HMPAM solutions. The increase was more pronounced once the concentration of HMPAM was in the semi-dilute regime and the concentration of NPs was larger than a critical threshold. The results suggest that in the semi-dilute regime, where polymer chains are in closer proximity to each other, NPs-induced bridging between HMPAM chains can occur which in turn enlarge the hydrodynamic radius of the hybrids and consequently increase their viscosity.

Experimental

Materials

GPTMS-modified silica NPs which are available under the commercial name Levasil CC301 were supplied by Akzo Nobel in suspension (ρ = 1.2 g cm^{-3}) containing 28.1 wt% silica with an average particle diameter of 7 nm as reported by the manufacturer. Bare silica NPs were supplied by Sigma-Aldrich in powder form with a particle diameter of 10–20 nm obtained from BET. Acrylamide and *t*-butyl acrylamide monomers were purchased from Sigma-Aldrich. HMPAM (98 mol% acrylamide and 2 mol% *t*-butyl acrylamide) and PAM (100 mol% acrylamide) were synthesised using free radical polymerization.[24] Their average molecular weights were estimated using the methodology used by Wu *et al.*[43] which is based on viscosity measurements and found to be approximately 2.1×10^6 and 2.7×10^6 g mol^{-1} for HMPAM and PAM respectively (see the ESI†). Sodium chloride (NaCl) and calcium chloride dihydrate ($CaCl_2 \cdot 2H_2O$) used for brine preparation were purchased from Sigma-Aldrich as well. All materials were used as received without further purification.

Preparation of modified silica NPs, polymers and hybrids

GPTMS-modified silica NPs. Detail of typical modification conditions and characteristics of GPTMS-modified silica NPs are described elsewhere.[39,44,45] Here, we highlight only the

important aspects. GPTMS is a silane epoxy functional group ($RSi(OMe)_3$) which is not stable in aqueous solutions. It undergoes a hydrolysis reaction according to the following chemical reaction:

$$RSi(OMe)_3 + 3H_2O \rightarrow RSi(OH)_3 + 3MeOH \quad (1)$$

Pre-hydrolysed silane is continuously added to the colloidal silica at 60 °C, at a rate of nearly 1.4 molecules GPTMS per nm^2 silica surface per hour while being agitated. The pre-hydrolysed silane reacts with silanol groups on the surface of silica NPs, according to the following condensation reaction:

$$Y\text{–}R\text{–}Si(OH)_3 + (HO)_X\text{–silica particle} \rightarrow Y\text{–}R(OH)_{3-X}\text{–silica particle} + xH_2O \quad (2)$$

An aqueous silica sol contains 4.6 silanol groups per nm^2 silica surface.[39] Since each silane reacts with three silanol groups and there exists 1.4 molecules GPTMS per nm^2, only 0.4 silanol groups per nm^2 remains on the surface, which shifts the surface from hydrophilic to hydrophobic.[46] During silylation, GPTMS covalently binds to the surface of silica and the epoxy ring opens and converts to a diol as indicated in Scheme 1a. The silylation of silica surface also substantially decreases the total of charged surface groups and specific surface area. The schematic of a GPTMS-modified silica nanoparticle is shown in Scheme 1b.

Polymers. Polymerization reactions of acrylamide monomers to synthesize PAM and acrylamide and *t*-butyl acrylamide monomers to synthesize HMPAM were performed in a double-walled glass sealed reactor with magnetic stirring coupled through the lid towards an internal propeller stirrer. The reactor was filled with a pre-set amount of monomers and de-ionised (DI) water. Thereafter, a water-cooled condenser was placed on the lid and the temperature was raised to 40 °C using an external thermostat connected to the lid. Subsequently, an inlet tube was lowered into the liquid phase, purging the water-monomer phase with nitrogen under stirring to remove any oxygen present. After 30 minutes of purging, the nitrogen tube was lifted into the headspace. Shortly after, 10 mL of DI water containing 0.05 mole potassium persulfate as the initiator was introduced through a septum to commence the polymerization. Viscosity was built up within 5–10 minutes; however, polymerization was allowed to run for two hours to complete the process. The original concentration of the solution of monomers was 5 wt%. The feed molar ratio of acrylamide to *t*-butyl acrylamide monomers in HMPAM was 98 to 2.

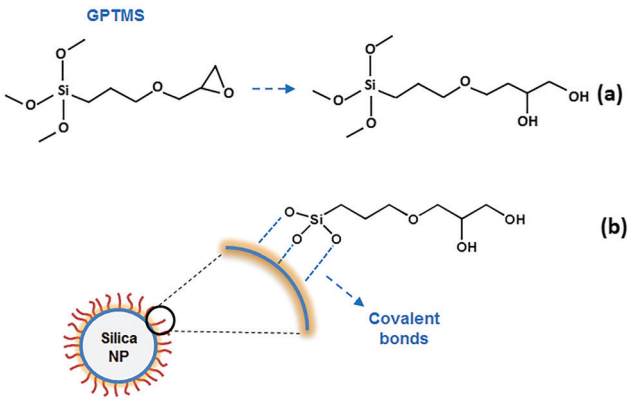

Scheme 1 (a) Ring-opening of GPTMS during silylation reaction. (b) The schematic of attachment of GPTMS to a silica nanoparticle surface by covalent bonds.

Hybrid samples. Hybrid samples were prepared by adding the required amounts of HMPAM and modified NPs in brine with a salinity of 20 wt% TDS including 1.5 wt% Ca^{2+}, hereafter referred to as Brine2015. Polymer solutions and NPs dispersions were diluted from their original concentration to the desired concentration in Brine2015 as the dispersant medium and stirred overnight and for 2 hours respectively until they became completely homogenous and transparent. In order to achieve a hybrid at desired concentration of polymer (C_p) and NPs (C_{np}), the required mass of NPs dispersion with a concentration of $2C_{np}$ was added to the equal mass of polymer solution with a concentration of $2C_p$. The hybrid sample was then homogenized by stirring for nearly 2 hours. In order to ensure the homogeneity and stability of the hybrid sample, it was stored for one week, in the absence of degrading factors such as light and heat, before viscosity measurements were made.

Characterization of NPs and HMPAM

Zeta potential. The zeta potential of the NPs in DI water was identified by means of a Malvern Zetasizer Nano ZS at room temperature. The NPs concentration was adjusted to provide a count rate of *ca.* 500 kcps on this instrument. Samples were run in triplicate in the auto mode and the average was recorded. There was a 30–60 seconds pause between each run, so the sample is able to relax. For GPTMS-modified silica NPs the zeta potential was measured to be -29 ± 5 mV.

Transmission electron microscopy (TEM). TEM imaging on the NPs was performed using a JEOL JEM 1400 TEM with a 120 kV beam. For preparing the samples, a 10 μL droplet of the NPs dispersion was brought into contact with the carbon grid. The sample droplet was slid off the grid after approximately 5 seconds of contact. The grid was then dried in ambient conditions for 5 minutes before inserting it into the TEM machine.

Determination of ligand grafting density. The number of moles of bound ligands per unit surface area (*i.e.* the grafting density σ) was experimentally derived from total organic carbon (TOC) analysis.[47] TOC analysis was performed using a DC-190 Dohrmann high temperature TOC Apparatus. A 100 μL sample was placed in the combustion tube. Catalytic oxidation of the sample in a furnace produced a gaseous mixture of CO_2 and H_2O. The CO_2 and steam were moved into the internal circulation reactor using a carbon-free carrier. Then, it passed through a condenser, a liquid gas separator and the moisture trap. The permeation dryer removed the H_2O. After that, the dried CO_2 passed through the non-dispersive infrared detector (NDIR) in order to measure the total carbon content. The grafting density from the TOC analysis was determined using eqn (3):[47]

$$\sigma = \frac{\frac{[C]}{[NP]}\rho_c \frac{4}{3}\pi R_c^3}{MW_1 4\pi R_c^2} \quad (3)$$

where [NP] represents the concentration of NPs, [C] is the organic carbon concentration obtained from TOC analysis, ρ_c and R_c are the density and radius of a nanoparticle respectively and MW_l is the molecular weight of GPTMS.

NMR elucidations. The prepared stock polymer solutions were freeze-dried by Christ Alpha 1-4 LD plus apparatus. The solutions were frozen quickly with liquid nitrogen in a glass flask, which was then attached to the freeze-dryer and left there overnight without further cooling. Thereafter, the obtained polymer powders were dissolved in D_2O. Before the test, air bubbles were removed by centrifuging the sample at 10 000 revolutions per minute (rpm) for 20 minutes. All spectra were recorded on a wide-bore 500 MHz Bruker NMR. ^{1}H NMR spectra were acquired at 500 MHz to determine the hydrophobic content of HMPAM. As a reference, a similar analysis was performed on PAM.

Rheological measurements. The viscosity of the polymer solutions, NPs dispersions and hybrid samples were measured by an Anton Paar rheometer (MCR-302) in Couette geometry. To investigate any shape memory effects, all measurements were done four times by repeating the sequence (a) from low to high shear rates and (b) then from high to low shear rates. It turned out that the four different series of viscosity data per sample were identical within the experimental error ($<5\%$). Hence, the average values of the viscosity of the four series were considered.

In order to study the shear-thinning behaviour of the polymer solutions, the Carreau–Yasuda model[48] as shown in eqn (4) was used:

$$\eta - \eta_\infty = (\eta_0 - \eta_\infty)[1 + (\dot{\gamma}\lambda)^a]^{\frac{n-1}{a}} \quad (4)$$

where η is the polymer viscosity, η_∞ denotes the viscosity of second Newtonian plateau which is assumed to be equal to the viscosity of the solvent, η_0 is the zero shear rate viscosity of the polymer, $\dot{\gamma}$ is the shear rate and λ is a time constant known as relaxation time which is an inverse of a critical shear rate at which the transition from Newtonian to shear-thinning regimes occurs. The parameter n is the power-law slope obtained from the shear thinning part and the parameter a controls the width of transition from Newtonian to shear thinning. For oscillatory tests, the amplitude sweep was attempted at a constant frequency to realize the linear viscoelastic regime after which the frequency dependence of the hybrids was analysed within this viscoelastic regime.

Colloidal stability of dispersed NPs

Inter-particle interactions. Dispersed NPs are subject to Brownian motion which induces frequent inter-particle collisions. The balance between inter-particle interactions determines whether the dispersion of NPs is stable. Inter-particle interactions between coated NPs have been successfully described by the xDLVO theory.[41,49] According to this theory, the total interaction between two functionalized spherical NPs (V_t) with radius R, at separation distance h is specified by the sum of van der Waals (V_{vdw}), electrostatic (V_{ele}), and steric (V_{str}) potentials:

$$V_t(x) = V_{vdw}(x) + V_{ele}(x) + V_{str}(x) \quad (5)$$

where x is the normalised separation distance equal to h/R.

The van der Waals potential is:[50]

$$\frac{V_{vdw}(x)}{k_B T} = -\left(\frac{\left(\sqrt{A_p} - \sqrt{A_m}\right)^2}{6k_B T}\right) \times \left[\frac{2}{x(x+4)} + \frac{2}{(x+2)^2} + \ln\left(\frac{x(x+4)}{(x+2)^2}\right)\right] \quad (6)$$

where A_p and A_m are Hamaker constants for particle and medium respectively,[51] k_B is the Boltzmann constant and T is the absolute temperature. The electrostatic potential is given by:[52]

$$\frac{V_{ele}(x)}{k_B T} = \frac{2\pi\varepsilon_0\varepsilon_r\psi_0^2 R}{k_B T}\ln\left(1 + e^{-\kappa R x}\right) \quad (7)$$

where ε_0 is the vacuum permittivity, ε_r is the medium relative permittivity, ψ_0 is the surface potential and κ^{-1} is Debye length. The latter is calculated as follows:

$$\kappa^{-1} = \left(\frac{\varepsilon_0\varepsilon_r k_B T}{2N_A e^2 I}\right)^{0.5} \quad (8)$$

where e is the electronic charge, N_A is the Avogadro number, and I is the medium ionic strength.[53] Surface potential is approximated by knowing the zeta potential (ζ) using eqn (9):

$$\psi_0 = \zeta\left(1 + \frac{1}{\kappa R}\right)e \quad (9)$$

The steric potential (V_{str}) for the grafted ligand is calculated by summing the osmotic (V_{osm}) and elastic potentials (V_{ela}).[53] These are short-range repulsive interactions that tend to kinetically stabilize the NPs dispersion. The osmotic potential can be expressed as:[54]

$$\frac{V_{osm}(x)}{k_B T} = \frac{4\pi RLN_A}{\nu_1}\phi_l^2\left(\frac{1}{2} - \chi\right)\left(1 - \frac{x}{2\alpha}\right) \quad \alpha \le x \le 2\alpha$$

$$\frac{V_{osm}(x)}{k_B T} = \frac{4\pi RL^2 N_A}{\nu_1}\phi_l^2\left(\frac{1}{2} - \chi\right)\left[\frac{x}{2\alpha} - \frac{1}{4} - \ln\left(\frac{x}{\alpha}\right)\right] \quad x < \alpha \quad (10)$$

where L is the particle coating thickness, α is equal to L/R, ν_1 is the solvent molar volume, ϕ_l is the ligand volume fraction (see the ESI†) and χ is the Flory–Huggins interaction parameter which is a function of solvent quality.[53] When the particle separation distance is shorter than the thickness of particle coating (*i.e.* $x < \alpha$) entropic effects arise from the compression of the ligand resulting in elastic repulsion between particles given by:[55]

$$\frac{V_{ela}(x)}{k_B T} = \left(\frac{2\pi RN_A}{MW_l}\phi_l L^2\rho_l\right)\left[\frac{x}{\alpha}\ln\left(\frac{x}{\alpha}\left(\frac{3 - \frac{x}{\alpha}}{2}\right)^2\right) - 6\ln\left(\frac{3 - \frac{x}{\alpha}}{2}\right) + 3\left(1 - \frac{x}{\alpha}\right)\right] \quad (11)$$

where ρ_l is the bulk density of the pure ligand. Dispersions of NPs stay kinetically stable if the potential barrier (V_{max}) is larger than $\sim 16/k_BT$.[56,57]

Results and discussion

Stability of hydrophobically modified silica NPs

Dispersions of GPTMS modified silica NPs in Brine2015 were found to be stable for over three months (Fig. S1, ESI†). In order to characterize the morphology of GPTMS-modified NPs (*i.e.* shape and size), TEM was performed for modified NPs dispersed either in DI water or in Brine2015. In order to study the impact of GPTMS modification on the prevention of aggregation of silica NPs, TEM was also performed on bare silica NPs with an approximately identical particle diameter (10–20 nm as reported by the supplier). Fig. 1 shows the TEM images of dilute dispersions of hydrophobically modified and bare silica NPs in DI water and in Brine2015. Stable dispersions were obtained for both types of NPs in DI water. However, the dispersion of modified NPs was completely transparent while the dispersion of bare NPs showed some turbidity (Fig. S2, ESI†). Fig. 1a shows that for the bare silica NPs in DI water, NPs formed aggregates even though the dispersion showed no phase separation. In contrast, for the GPTMS-modified NPs dispersed in DI water the TEM image (Fig. 1b) shows the presence of individual NPs and small clusters of NPs with a narrow cluster size distribution (see Fig. S5, ESI†) suggesting a slight tendency of NPs to form large aggregates.

When bare NPs were dispersed in Brine2015 most of them adhered to one another and large aggregates were formed (see Fig. 1c). This is in agreement with the flocculation of small silica NPs into particulate networks, resulting in sedimentation as also reported by others.[58,59] Fig. 1d shows that for GPTMS-modified silica NPs in Brine2015, even though a few slightly larger agglomerates were formed, a majority of the NPs remained separated from each other. This shows that grafting low molecular weight ligands to the surface of NPs can prevent their aggregation in media with high ionic strength.[47,60] The sample pictures of a suspension of bare and modified silica NPs in DI water and Brine2015 at a concentration of 0.05 wt% are shown in Fig. S2 (ESI†).

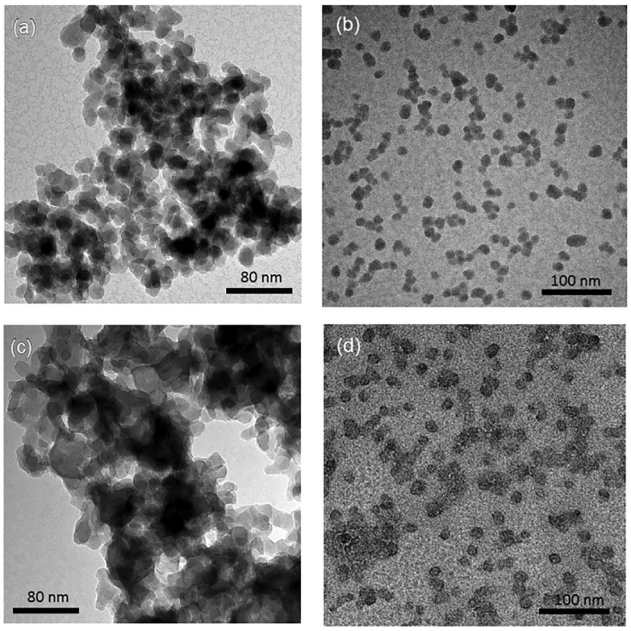

Fig. 1 TEM images of dried samples (a) bare NPs in DI water (b) GPTMS-modified NPs in DI water (c) bare NPs in 20 wt% TDS brine (Brine2015) and (d) GPTMS-modified NPs in Brine2015.

To determine the relative contributions of the surface forces to NPs interactions, the van der Waals, electrostatic and steric potentials were estimated using the xDLVO theory (see Interparticle interaction section). This provides a semi-quantitative description of stability of NPs and the calculations highlight the importance of the grafted ligand for NPs stabilization at high salinity. For this purpose, three scenarios were considered: (a) bare silica NPs dispersed in a medium with low ionic strength (I = 10 mM, equivalent to 0.06 wt% NaCl), (b) bare silica NPs in a high ionic strength medium (I = 3834 mM representing the ionic strength of Brine2015) and (c) GPTMS modified NPs in a medium with similar high ionic strength. Table 1 summarises the parameters which were used for the calculations. All three scenarios were considered at room temperature. The ligand grafting density from TOC analysis according to eqn (3) was calculated to be 2.6 ± 0.1 μmol m^{-2}. The thickness of the particle coating (L) was regarded as the length of a GPTMS molecule which is 0.95 nm.[60] Even though it is reported in the literature that GPTMS is relatively well solvated in high salinities water,[39,60] the Flory–Huggins interaction parameter was taken as 0.49 to give a conservatively low estimate of V_{osm}.

The calculated interaction potentials are shown in Fig. 2. As Fig. 2a suggests, for bare silica NPs dispersed in a low ionic strength medium, V_{ele} decreased exponentially with increasing h, approaching zero at large h. V_{vdw}, which indicates an inverse power law with h, did not decay to zero. V_{vdw} is dominant over V_{ele} in very short particle separation distances, which results in a deep minimum in the V_t profile. However, for larger h values (*i.e.* $h > 0.1$ nm), the electrostatic double layer repulsion becomes dominant and a potential barrier of larger than $55/k_BT$ is obtained ($V_{max} > 55/k_BT$). This implies that the colloidal stability is ensured. When bare silica NPs were dispersed in Brine2015 (Fig. 2b), V_{vdw} did not change, as it is

Table 1 Functionalised NP parameters at 298.15 K used in xDLVO theory calculations

Parameter	NPs functionality
Hamaker constant for water (J)	3.7×10^{-20}
Hamaker constant for silica (J)	6.3×10^{-20}
Particle diameter (nm)	7
Bulk density of ligand (g cm^{-3})	1
Ligand molecular weight (g mol^{-1})	236
Ligand grafting density (μmol m^{-2})	2.6
Ligand length (nm)	0.95
ζ potential (mV)	−29
Flory–Huggins interaction parameter	0.49

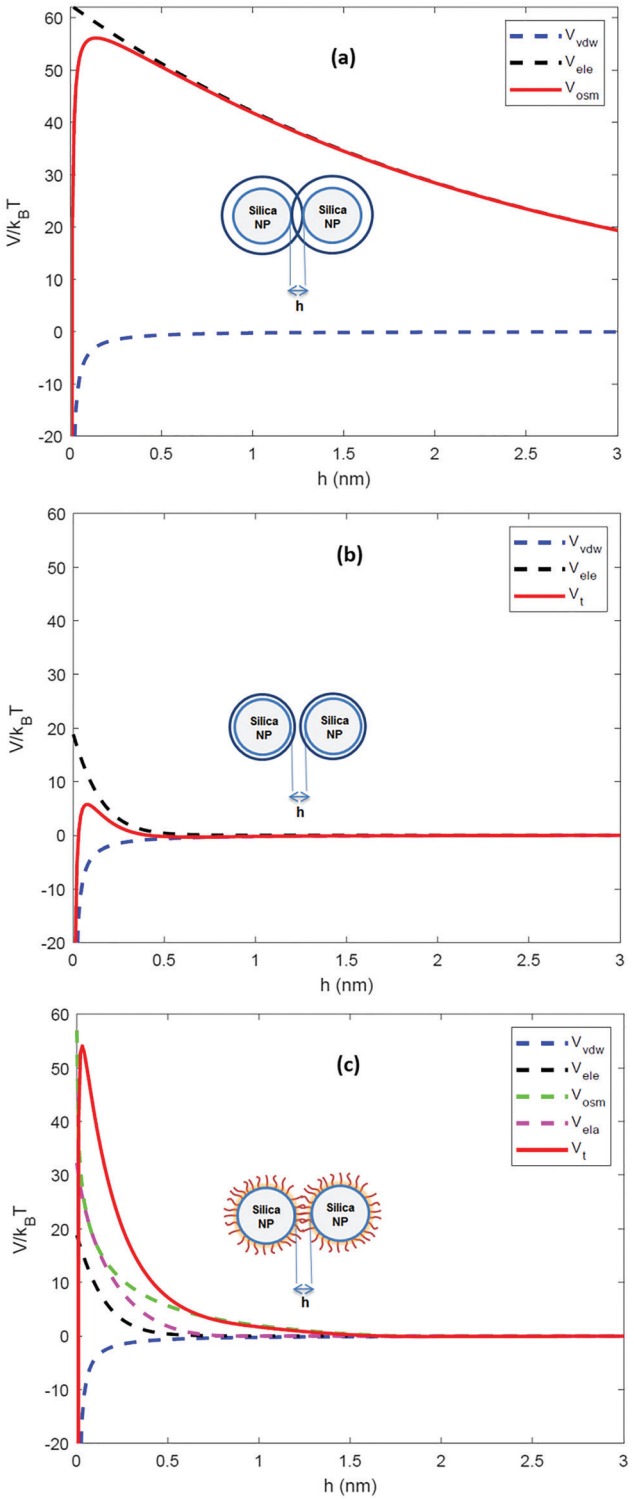

Fig. 2 Inter-particle interaction potential (V) as a function of particle separation distance (h) calculated by xDLVO theory for (a) un-modified NPs in a medium with low ionic strength (I = 10 mM) (b) un-modified NPs in a medium with high ionic strength (I = 3834 mM) and (c) GPTMS-modified NPs in same high ionic strength medium.

independent of aqueous phase salinity. However, as can be inferred from eqn (8), the Debye length diminishes with increasing ionic strength, resulting in significant reduction in V_{ele}. This is also evident in V_t and the potential barrier becomes smaller than $16/k_BT$ ($V_{max} < 16/k_BT$) implying that the colloidal stability is not achieved. The fact that the potential barrier did not completely disappear was due to the high ζ potential and small size of the NPs. The latter makes the van der Waals attracting potential smaller.

When two GPTMS-modified silica NPs approach each other to a separation distance h smaller than $2L$ ($h < 2L$) the ligand molecules interact with each other, which leads to an increase in the local segment density of ligand molecules in the interaction zone. This results in strongly repulsive interaction due mainly to two effects: (a) to rise in osmotic potential in the interaction zone according to eqn (10) and (b) decrease in configurational entropy of the ligand molecules in the overlap region due to decrease in volume available for ligand molecules, as is shown in eqn (11). Fig. 2c indicates that the contribution of V_{osm} and V_{ela} significantly increases the potential barrier to more than $50/k_BT$ ($V_{max} > 50/k_BT$) which ensures the colloidal stability of GPTMS-modified silica NPs at such high salinity. Note that these calculations are based on some inherent assumptions in xDLVO theory[61] and were used to semi-quantitatively show the effect of NPs surface modification by GPTMS on the colloidal stability of the system.

Hydrophobic content of HMPAM

The result of ^{1}H NMR spectra is shown in Fig. 3. For PAM, as can be seen in Fig. 3a, peaks a and b correspond to aliphatic CH_2 and aliphatic CH respectively in polyacrylamide. Moreover, some other peaks appear in the range of 5.65–6.25 ppm. These peaks are attributed to vinylic CH and CH_2 in acrylamide monomer which means some of the monomers were not polymerized.[62] The yield of polymerization was estimated to be 92.5 ± 0.5%. For HMPAM, as can be seen in Fig. 3b, compared with PAM two additional peaks were detected. Peak c corresponds to the proton in the methyl group (–$(CH_3)_3$) of HMPAM. Another peak (c′) was observed next to peak c. This small peak is attributed to the methyl groups in *t*-butyl acrylamide monomer which were not polymerized (see the ^{1}H NMR spectrum of *t*-butyl acrylamide in Fig. S8, ESI†). Also here, the peaks in the range of 5.65–6.25 ppm correspond to vinylic CH and CH_2 in acrylamide and *t*-butyl acrylamide monomers which were not polymerized. As compared to PAM, the integrating areas of these peaks appear to be larger. This indicates that the yield of the polymerization is smaller and it was estimated to be 81.0 ± 0.5%.

The hydrophobic content of HMPAM was estimated according to the following equation:

$$\frac{S_c}{S_a + S_b} = \frac{9z}{3y + 3z} \quad (12)$$

where S_a, S_b, and S_c are the integrating areas of peaks a, b and c respectively, and y and z are the non-hydrophobic and hydrophobic content of HMPAM respectively ($y + z = 100$). This leads to

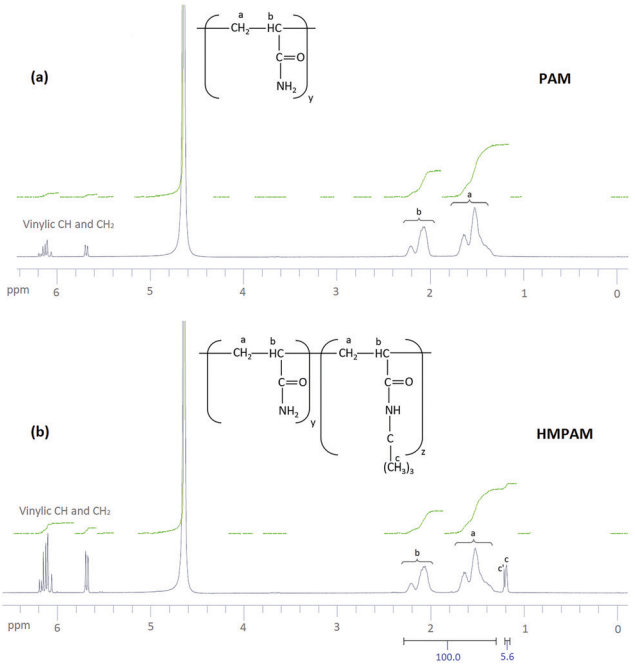

Fig. 3 ^{1}H NMR spectra of (a) PAM and (b) HMPAM. Peaks a and b correspond to aliphatic CH_2 and aliphatic CH respectively in PAM and HMPAM. Peak c corresponds to the proton in the *t*-butyl group of *t*-butyl acrylamide in HMPAM. Peak c′ corresponds to *t*-butyl group in *t*-butyl acrylamide monomers which were not polymerized. For HMPAM the sum of integrating areas of peaks a and b is 100 and the integrating area of peak c is 5.6.

a hydrophobic content of 1.80 ± 0.05 mol% which is slightly smaller than the hydrophobic content in the original feed.

Rheology of HMPAM solutions

Fig. 4 shows the viscosities of HMPAM solution in DI water and in Brine2015 at 25 °C and in Brine2015 at 70 °C as a function of shear rate at different concentrations. The Carreau–Yasuda model (eqn (4)) was used to fit the experimental rheology data. The list of fitting parameters is tabulated in Tables S1–S3 (ESI†). From Fig. 4a it can be observed that HMPAM solutions in DI water showed a Newtonian behaviour at low to intermediate shear rates which was followed by a shear thinning behaviour at higher shear rates. The extension of the Newtonian and shear-thinning regimes depends on the concentration of HMPAM. The shear-thinning effect was more pronounced for high concentrations of HMPAM solution. This is explained by the deformation of polymer chains in the shear direction, which allows for easier flow of the molecules, resulting in the reduction of the viscosity with an increase in shear rates.[63] However, it was found that at concentrations lower than 0.1 wt%, HMPAM solution only exhibits a Newtonian behaviour over the range of tested shear rates. This suggests that, in this case, the structural characteristics of the polymer chains no longer affect the viscosity. The shear rate dependency of HMPAM solution increased with an increase in polymer concentration. This is ascribed to an increase of associations among polymer chains leading to the higher viscosity and extending the shear thinning

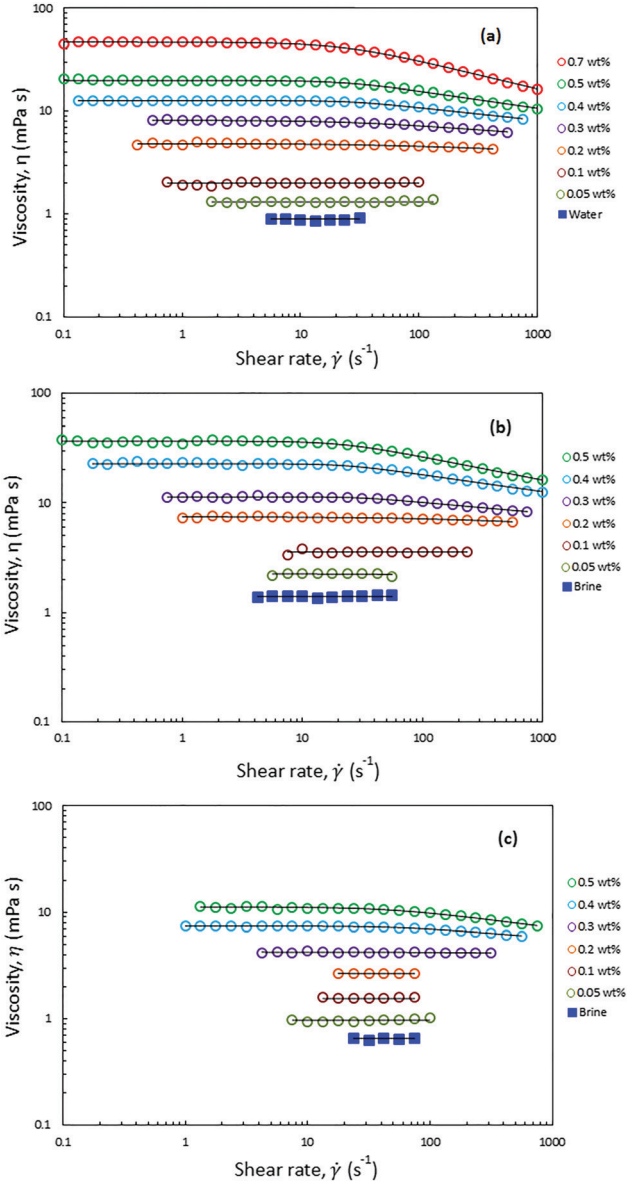

Fig. 4 Steady state shear viscosity of HMPAM at different concentrations in (a) DI water at 25 °C (b) Brine2015 at 25 °C and (c) Brine2015 at 70 °C. The solid line is acquired by fitting the experimental data into Carreau–Yasuda model. The fitting parameters are presented in Tables S1–S3 (ESI†).

region.[64] Such shear rate dependency was more pronounced at concentrations larger than the overlap concentration (C_p^*), which was calculated to be approximately 0.49 ± 0.01 wt% for HMPAM in DI water (see Fig. S7a, ESI†). From Table S1 (ESI†) it can be seen that relaxation time increases as concentration rises. This means that at higher concentrations, when HMPAM molecule is deformed by shear forces, it requires a longer time to relax to its original conformation.

HMPAM showed an excellent solubility in Brine2015 over the range of tested concentrations, up to 0.5 wt%, which led to complete transparent solutions. Since HMPAM is a non-ionic polymer, it did not strongly respond to the presence of cations in the solvent. Fig. 4b shows that, irrespective of concentration,

the viscosity of HMPAM solutions increased in Brine2015 throughout all the tested shear rates as compared to HMPAM solutions in DI water. As HMPAM showed an excellent solubility both in DI water and Brine2015, this is mainly attributed to an increase in solvent viscosity which was measured to be 0.9 ± 0.1 and 1.4 ± 0.1 mPa s for DI water and Brine2015 respectively. This implies that the increase in viscosity is approximately 55% which is close to the observed increase in the viscosity for HMPAM at various concentrations. The overlap concentration of HMPAM dissolved in Brine2015 was found to be approximately 0.30 ± 0.01 wt% (see Fig. S7b, ESI†). This infers that an association among HMPAM chains occurs at lower concentrations in Brine2015 than in DI water. As can be seen in Fig. 4b and Table S2 (ESI†), it was also found that at a given concentration, the shear-thinning behaviour was more pronounced and the relaxation time was longer in Brine2015 when compared with HMPAM in DI water. Fig. 4c shows that increasing the temperature from 25 °C to 70 °C reduced the viscosities of HMPAM solution in Brine2015 and made the shear dependency of concentration less pronounced. Such a reduction in the viscosity was by a factor of 2.3 for HMPAM solutions with concentrations of 0.05 and 0.1 wt%, which is comparable with the reduction in viscosity of Brine2015. At higher concentrations, this factor increased up to 3.3 for 0.5 wt% HMPAM.

Rheology of HMPAM–NPs hybrids at high salinity and temperature

The rheological response of the hybrids of HMPAM and GPTMS-modified NPs at high salinity and elevated temperature was investigated at various HMPAM and NPs concentrations. All the samples were prepared in Brine2015 and the viscosity measurements were performed at 70 °C. The concentration of HMPAM was selected as 0.05, 0.1 and 0.2 wt% in the dilute regime, 0.3 wt% in the boundary of transition from dilute to semi-dilute and 0.5 and 0.6 wt% in the semi-dilute regime. The concentration of NPs also varied from 0.5 to 4 wt%. Fig. 8 shows the results of such viscosity measurements. All the reported viscosities are at shear rate of reported viscosities are at shear rate of 7.5 s^{-1} which is within the typical range of practical shear rate values in various industrial processes.[65] The inserted values on the horizontal axis of the plot in Fig. 5 correspond to the viscosities of HMPAM solutions without NPs. The viscosity of Brine2015 at 70 °C (corresponding to the origin of the graph) was 0.6 ± 0.1 mPa s. Once up to 0.3 wt% of HMPAM was added to Brine2015, the viscosity increased to 4.2 ± 0.1 mPa s. An additional increase of the concentration to 0.5 and 0.6 wt% significantly increased the viscosity to 11.2 ± 0.1 and 19.5 ± 0.1 mPa s respectively as the association among chains was achieved. The values along the vertical axis of the plot in Fig. 5 represent the viscosity of NPs dispersion in the absence of HMPAM. The increase in NPs concentration from 0.5 to 4 wt% increased the viscosity from 0.6 ± 0.1 to 1.0 ± 0.1 mPa s. The viscosity of HMPAM–NPs hybrids is discussed at different polymer concentration regimes. In the dilute regime (C_p = 0.05, 0.1 and 0.2 wt%), the addition of NPs to

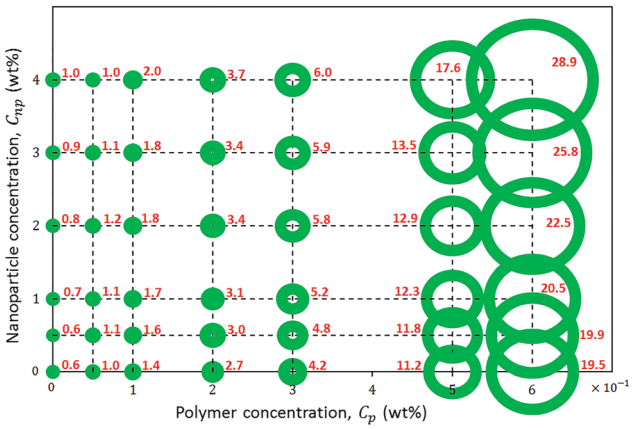

Fig. 5 Viscosities of HMPAM–NPs hybrids at shear rate of 7.5 s^{-1} at different concentrations. The materials were dispersed in Brine2015 and the measurements were done at 70 °C. The magnitude of viscosity in terms of mPa s is shown next to or inside the circle. The viscosities scale with radius of the circles.

HMPAM solution did not have a substantial impact on the viscosity of the hybrids. For instance, the addition of 4 wt% NPs to 0.2 wt% HMPAM only increased the viscosity another 1.0 ± 0.1 mPa s. Once the HMPAM concentration was close to the overlap concentration (C_p = 0.3 wt%), as the NPs concentration increased, a more substantial increase in viscosity was perceived (incremental viscosity of 1.8 ± 0.1 mPa s with the addition of 4 wt% NPs). Furthermore, in the semi-dilute regime (C_p = 0.5 and 0.6 wt%) the most significant synergic effect was witnessed. Addition of 4 wt% NPs to 0.5 and 0.6 wt% HMPAM solution increased the viscosity another 6.4 ± 0.1 and 9.4 ± 0.1 mPa s respectively. In this polymer concentration regime, there appears to be a critical NPs concentration ($C_{np,c}$) present, above which the increase in the viscosity of the hybrid is more pronounced.

In order to provide a better assessment of the effect of $C_{np,c}$ on the viscosity of the HMPAM–NPs hybrid when HMPAM is in the semi-dilute concentration regime, Fig. 6 was plotted. The viscosity measurement was also attempted for the hybrid of 0.5 wt% HMPAM and 3.5 wt% NPs (this was not represented in Fig. 5 for better readability of the graph). As can be seen in

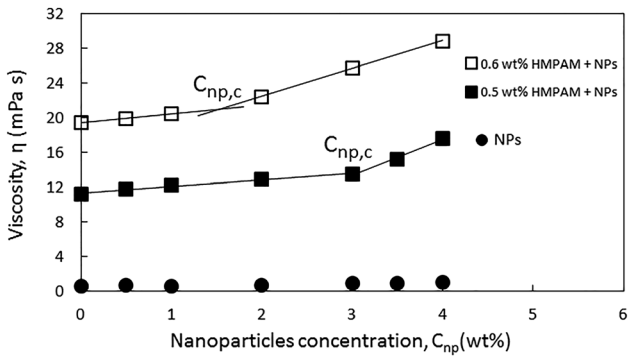

Fig. 6 Viscosities of 0.5 and 0.6 wt% HMPAM in combination with NPs at different concentrations ranging from 0 to 4 wt% at shear rate of 7.5 s^{-1}.

Fig. 6, regardless of concentration, the viscosity of the dispersion of NPs remained low, suggesting that the viscosity enhancement of HMPAM–NPs hybrid cannot be considered as a superposition of viscosity of HMPAM solution and NPs dispersion. On the other hand, the increase in NPs concentration increased the viscosity of the hybrids containing 0.5 and 0.6 wt% HMPAM in two different regimes: for the hybrids containing 0.5 wt% HMPAM, with the addition of up to 3 wt% NPs, the viscosity of hybrid grew linearly with a relatively small growth rate; however, from 3 wt% to 4 wt% a second more significant linear increase in viscosity was observed. This suggests that in order to have a considerable increase in the viscosity of the hybrid, the NPs concentration should be above a certain critical threshold ($C_{np,c}$) to bridge between HMPAM chains using hydrophobic–hydrophobic interactions. $C_{np,c}$ for the hybrids containing 0.5 wt% HMPAM was 3.0 ± 0.1 wt%. For the hybrid containing 0.6 wt% HMPAM, however, it was found that $C_{np,c}$ is lower (1.5 ± 0.1 wt%). This can be explained by the fact that with an increase in the HMPAM concentration in the semi-dilute regime, the polymer chains come in closer proximity to each other and a smaller amount of NPs is needed to enable the bridging between HMPAM molecules.

To investigate the influence of hydrophobic–hydrophobic interactions on the NPs-induced bridging between HMPAM molecules, the shear rate dependency of two combinations were studied (a) the hybrid of 0.5 wt% HMPAM and 4 wt% NPs and (b) the hybrid of 0.5 wt% PAM and 4 wt% NPs. As mentioned earlier, unlike HMPAM, PAM does not contain the hydrophobic group of *t*-butyl acrylamide and it was selected to examine whether there is a similar synergic effect between PAM and NPs or not. As can be seen in Fig. 7, the viscosity of the hybrid of HMPAM and NPs is considerably higher than the viscosity of HMPAM, whereas a synergic effect was not observed for the hybrid of PAM and NPs and the viscosity of this hybrid was only slightly higher than the viscosity of PAM. This finding suggests that NPs can facilitate the bridging between HMPAM molecules only using hydrophobic–hydrophobic interactions, with the end result of creating larger molecules, whereas such an effect was not observed for the hybrid of NPs and PAM. Therefore, it can be inferred that as expected there is no effective interaction between PAM and hydrophobically modified silica NPs.

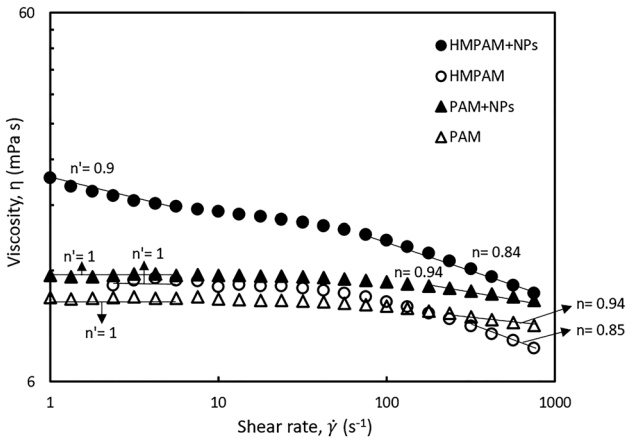

Fig. 7 Viscosities of polymer–NPs in Brine2015 at 70 °C as a function of shear rate. Open and filled circles represent viscosity of 0.5 wt% HMPAM and hybrid of 0.5 wt% HMPAM and 4 wt% NPs respectively. Open and filled triangles represent viscosity of 0.5 wt% PAM and hybrid of 0.5 wt% PAM and 4 wt% NPs respectively. n and n' represents the power-law slope at low and high shear rates respectively.

Moreover, to investigate the rheological properties of the hybrids, where shear-thinning occurs, the shear rate dependency of the hybrids was studied. As can be seen in Fig. 7, the hybrid of HMPAM and NPs showed a shear-thinning behaviour both in low shear rates ($<10\ s^{-1}$) and high shear rates ($>100\ s^{-1}$). The power-law slope of the second shear-thinning is close to the power-law slope of the shear-thinning observed for HMPAM at high shear rates, whereas at low shear rates we did not detect a shear-thinning for HMPAM. We hypothesize the presence of two shear-thinning regimes for HMPAM–NPs hybrid as follows. HMPAM chains are bridged by NPs through two types of interactions between HMPAM chains and NPs; weak interactions and strong interactions. When the hybrid is exposed to a shear-flow field, first at low shear rates, the weak interactions are continuously broken which results in the first shear-thinning regime. In intermediate shear rates, only strong interactions play a role in NPs-induced bridging between HMPAM chains which are not yet broken. As a result, a Newtonian regime is observed for the HMPAM–NPs hybrid at intermediate shear rates. At high shear rates, however, strong interactions are also broken which leads to the second shear-thinning regime. It should be noted that the hybrid of PAM–NPs did not show a shear-thinning behaviour at low shear rates which is again an indication of lack of effective interactions between PAM and NPs.

The shear-thinning behaviour was also investigated in different HMPAM concentration regimes. The selected hybrids contained constant NPs concentration of 4 wt% and the concentration of HMPAM varied from 0.2 to 0.6 wt% (*i.e.* from dilute to the semi-dilute regime). As can be seen in Fig. 8, at low shear rates, for the hybrids with HMPAM in the dilute regime, there was no shear-thinning regime, whereas for the hybrids with HMPAM in the semi-dilute regime we observed a shear-thinning behaviour and the power-law slope was around 0.9 (0.9 and 0.89 for 0.5 and 0.6 wt% HMPAM respectively). At high shear rates, for the hybrids with HMPAM in the dilute regime, the power-law slope was close to unity (1 and 0.96 for 0.2 and 0.3 wt% respectively), whereas when HMPAM was in the semi-dilute regime, the power-law slope was around 0.8 (0.84 and 0.81 for 0.5 and 0.6 wt% respectively). This increase in the power-law slope of the hybrids from dilute to semi-dilute regime is attributed to bridging between different HMPAM chains by NPs in the semi-dilute regime. In a shear-flow field, these bridges are broken and a more shear-thinning behaviour is expected. Formation of such bridges in the dilute regime is not expected as the HMPAM chains are not in close proximity of each other.

Dynamic rheological behaviour of the hybrids at different NPs concentration

In order to shed light on the viscoelastic response of HMPAM–NPs hybrids, the dynamic viscoelasticity was examined. For this

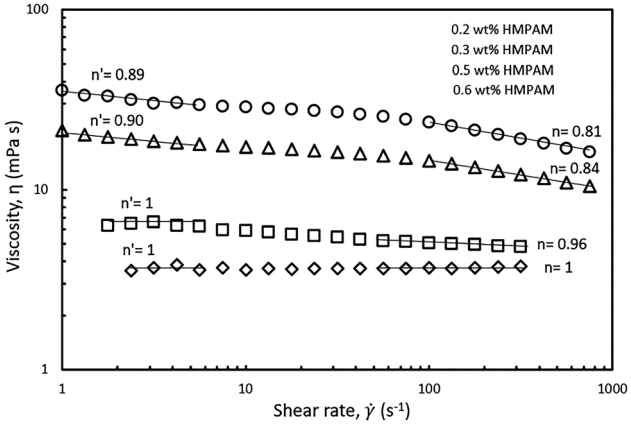

Fig. 8 Shear rate dependency of HMPAM–NPs hybrids in Brine2015 at 70 °C. The concentration of NP was kept constant at 4 wt% and the concentration of HMPAM varied from 0.2 to 0.6 wt%. Power-law slope decreased with increasing HMPAM concentration. n and n' represents the power-law slope at low and high shear rates respectively.

purpose two oscillatory tests were performed: (i) the amplitude sweep test to measure the storage modulus (G') and loss modulus (G'') as a function of strain (ε) and (ii) the frequency sweep test to assess the frequency dependence of the storage and loss moduli. The hybrids for which this analysis was performed contained constant NPs concentration of 4 wt% and the concentration of HMPAM varied from 0.2 to 0.6 wt% (*i.e.* from dilute to semi-dilute regime). This was to investigate the viscoelastic response of the hybrids in the different HMPAM concentration regimes.

As can be seen in Fig. 9a and b, for the amplitude sweep test performed on the hybrids, the loss modulus is larger than the storage modulus over the range of strains up to 1000% regardless of HMPAM concentration, implying that even for HMPAM in the semi-dilute regime the rheological response of the hybrids is controlled by the viscous component. The loss modulus was almost constant for the hybrids with 0.2 and 0.3 wt% HMPAM (*i.e.* when the polymer is in the dilute regime) but it slightly decreased for hybrids containing 0.5 and 0.6 wt% HMPAM (*i.e.* when the polymer is in the semi-dilute regime) at high strains. The storage modulus of these hybrids, however, showed a sharper decrease at high strains (note that accurate values of storage modulus were not measured for the hybrid with 0.2 wt% HMPAM at low and high strains due to the limitations of the rheometer). The stronger decrease of the storage modulus for these hybrids as compared to hybrids with HMPAM in the dilute regime is an indication of more effective interaction between HMPAM and NPs.

Fig. 9c shows that for all the tested frequencies, from 1 to 100 rad s^{-1}, all the hybrids exhibited predominantly viscous behaviour over elastic behaviour irrespective of HMPAM concentration. It can be seen that with the increase in HMPAM concentration, G' and G'' became stronger. The slope of G' over the slope of G'' in a log–log plot was calculated for these four hybrids. It was found that for the hybrids containing 0.2 and 0.3 wt% HMPAM (*i.e.* dilute regime) the slope ratio was

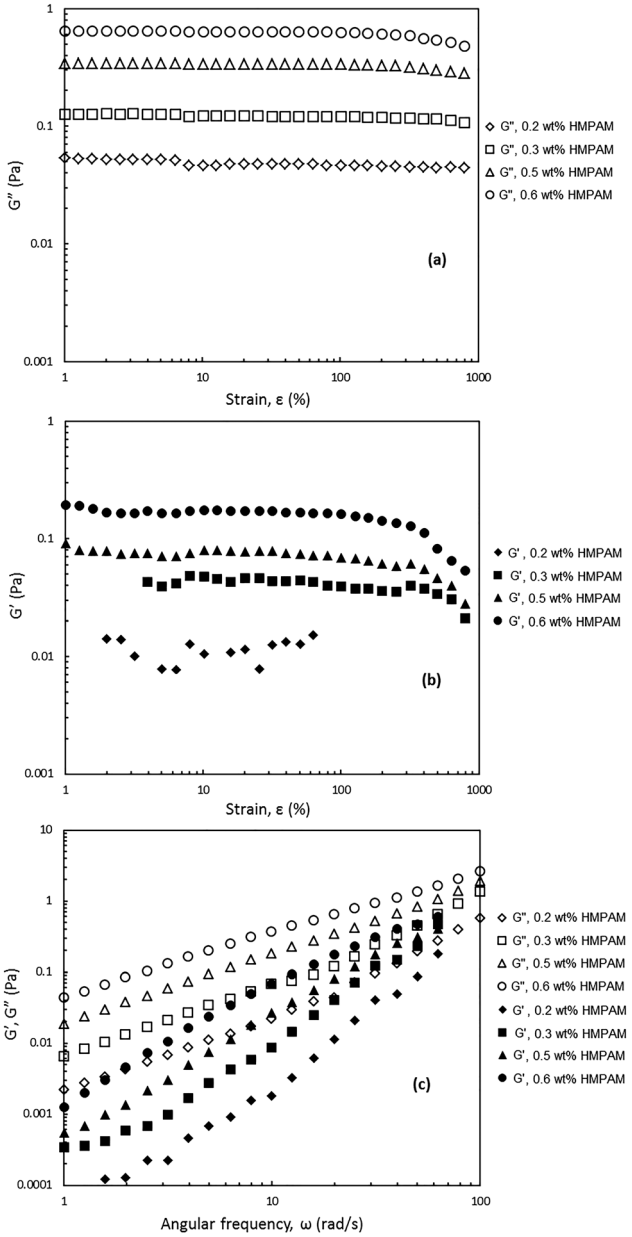

Fig. 9 Amplitude and frequency sweep tests. (a) Loss modulus G'' as a function of strain ε at constant angular frequency ω = 20 rad s^{-1}. (b) Storage modulus G' as a function of ε at constant ω = 20 rad s^{-1}. (c) G' and G'' as a function of ω at constant ε within the linear viscoelastic regime (ε was selected in the range of 50–75% depending on the test). Filled and open symbols represent G' and G'' respectively. The concentration of NPs was kept constant at 4 wt%. The concentration of HMPAM varied: diamonds, squares, triangles and circles represents HMPAM concentration of 0.2, 0.3, 0.5 and 0.6 wt% respectively.

2.0 ± 0.1 and 1.9 ± 0.1 Pa s rad^{-1} respectively indicating the hybrids behave like a liquid. Nonetheless, for the hybrids containing 0.5 and 0.6 wt% HMPAM (*i.e.* semi-dilute regime) the slope ratio was 1.7 ± 0.1 and 1.6 ± 0.1 Pa s rad^{-1} respectively. This decrease in slope ratio with increasing HMPAM concentration indicates that in the semi-dilute regime some degree of bridging between HMPAM chains induced by NPs occurs.

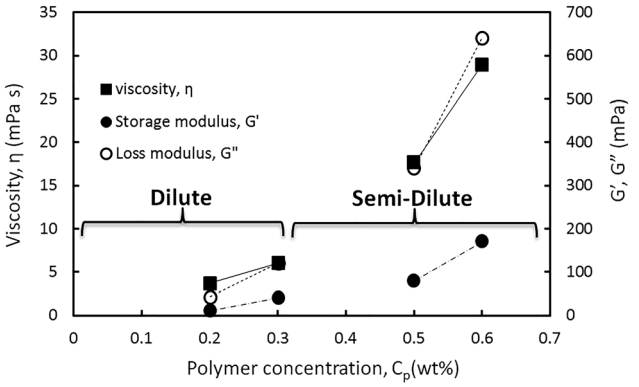

Fig. 10 Comparison of the viscosity and storage and loss moduli of the hybrids at constant NPs concentration of 4 wt% and varying HMPAM concentration from 0.2 to 0.6 wt%. G' and G'' were obtained from amplitude sweep test and constant angular frequency of 20 rad s^{-1}.

In Fig. 10 the viscosity and storage and loss moduli of the hybrids are plotted within the linear viscoelastic regime. This regime was obtained from the amplitude sweep test at a constant angular frequency of 20 rad s^{-1} in different HMPAM concentration regimes from dilute to semi-dilute. As can be observed for all three parameters the slope of the data points obtained in the semi-dilute regime became larger than their slope in the dilute regime. It can be concluded that the addition of 4 wt% NPs to HMPAM has a stronger viscoelastic effect when HMPAM is in the semi-dilute concentration regime.

To illustrate various interactions in HMPAM–NPs hybrids, the molecular scenario as indicated in Fig. 11 was drawn. The distribution of hydrophobic groups on HMPAM is random and HMPAM chains have a radius of gyration of approximately 80 ± 5 nm (see eqn (S4) in the ESI†), while the size of silica NPs is approximately 7 nm. The contour length of HMPAM was estimated to be 9.9 ± 1.9 μm which is much larger than the estimated persistence length of 2.2 ± 0.6 nm (see eqn (S5) in the ESI†). Therefore, our long-chain polymer behaves like a random coil. As indicated in Fig. 11a, for HMPAM chains in the semi-dilute regime in absence of NPs, two types of interactions are possible: (a) intra-chain hydrophobic association within an HMPAM chain (orange circles) and (b) inter-chain hydrophobic association between HMPAM chains (red circles). Fig. 11b represents the interaction of hydrophobic groups on HMPAM and hydrophobically modified silica NPs and how silica NPs can play as bridging sites between the HMPAM chains. As discussed before, based on the viscosity results, bridging between HMPAM chains occurs only when the concentration of NPs is above $C_{np,c}$. At concentrations lower than $C_{np,c}$, hydrophobic groups present in the HMPAM are anchored onto hydrophobically modified NPs and there are no free NPs in the dispersant. Nonetheless, beyond the $C_{np,c}$, free NPs come to be available and a further increase in C_{np} will result in bridging between different HMPAM chains by NPs (black circle). The existence of the $C_{np,c}$ is in agreement with observations of Hu *et al.*[36] and Zhu *et al.*[38] who argued that interaction between polymer and silica NPs occurs by hydrogen bonding. It should be noted that the reason why the synergic

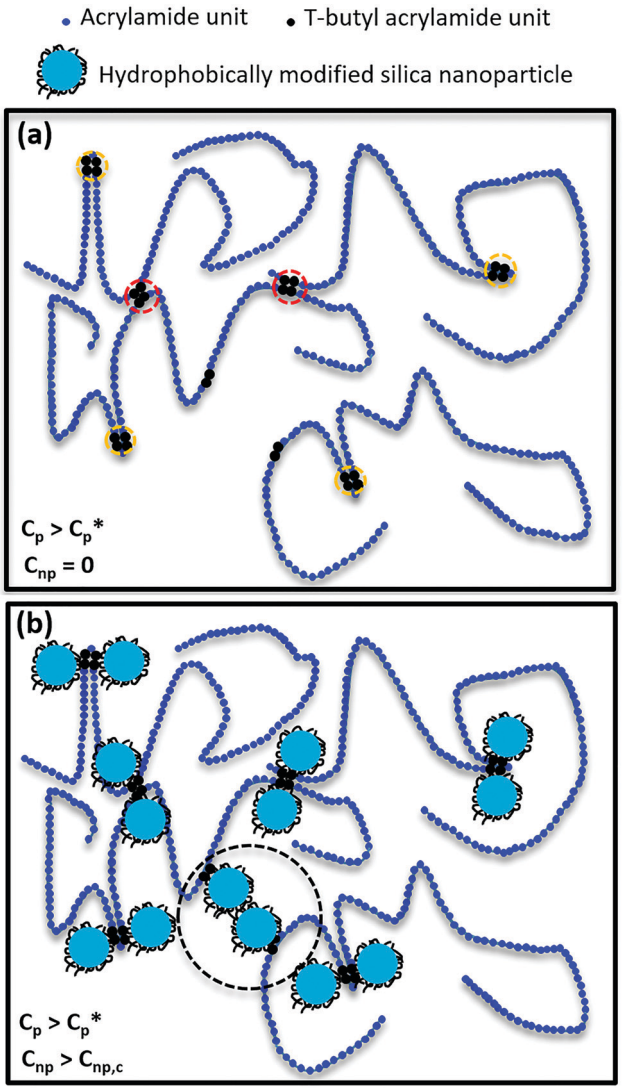

Fig. 11 Schematic of various interactions in HMPAM–NPs hybrids. (a) Intra-chain (orange circles) and inter-chain (red circles) hydrophobic associations in HMPAM chains in the semi-dilute regime in absence of NPs. (b) Bridging of HMPAM chains by NPs (black circle) in the semi-dilute regime when the concentration of NPs is larger than $C_{np,c}$.

effect between HMPAM and NPs is more significant when $C_p > C_p^*$, is because the inter-chain association between some HMPAM chains has occurred previously and the chains are in closer proximity to each other. Consequently, the probability of bridging between HMPAM chains by NPs becomes higher compared to the dilute regime where HMPAM chains are distant from each other. As a result of bridging between HMPAM chains, the movement of HMPAM chains is limited and the hydrodynamic radius of the hybrid increases which eventually results in an increase in the viscosity.

It should be noted that regardless of the concentration of HMPAM and NPs, all the developed hybrids were transparent and no phase separation was observed (see Fig. S3, ESI†). This demonstrates an important aspect of HMPAM–NPs hybrid as an alternative for conventional cEOR polymers at harsh

conditions as the enhanced stability is achieved. As long-term thermal stability is another imperative aspect of water-soluble polymers for cEOR, further complementary experiments such as the study of the colloidal stability and change in the hybrids viscosity over time are recommended to investigate the effectiveness of the hybrids at high temperature in a long-term.

Conclusions

We investigated an innovative hybrid system using a combination of a hydrophobically modified polyacrylamide (HMPAM) and hydrophobically modified silica nanoparticles (NPs). This system exhibited enhanced stability in high total dissolved solids (TDS) content and high hardness brines and improved the rheological properties of HMPAM at elevated temperatures. The silica NPs that had been modified by grafting an organic ligand (gamma-glycidoxypropyltrimethoxysilane) onto their surface showed good colloidal stability against aggregation at high salinity, due to the increased potential barrier as compared to bare silica NPs. Viscosity measurements at different HMPAM and NPs concentrations showed that the improved rheological behaviour was more pronounced when the concentration of HMPAM was more than the overlap concentration ($C_p^* \sim 0.3$ wt%). This occurred because in the semi-dilute regime HMPAM chains are in closer proximity and they can be bridged by NPs which in turn increases the hydrodynamic radius of the hybrid. Results also showed that for a given concentration of HMPAM in the semi-dilute regime, there was a critical concentration of NPs above which the bridging between HMPAM chains by NPs occurred and increased the viscosity more substantially. Dynamic rheological tests indicated that the hybrids were viscous dominated and storage and loss moduli had a stronger increase with HMPAM concentration in the semi-dilute regime compared to the dilute regime due to NPs-induced bridging between HMPAM chains. The results of this study provide insights into the interaction of polymer molecules and NPs in hybrid systems with the end result of enhancing the stability and improving the rheological properties, thus opening a pathway for developing other polymer-based systems for use in harsh conditions.

Conflicts of interest

The authors declare no conflict of interest.

Acknowledgements

This study is the result of collaboration between Delft University of Technology, The Netherlands Organisation for Applied Scientific Research (TNO) and Kuwait Oil Company. We are grateful to Kuwait Oil Company for funding this project. We are grateful to Filip Neele (TNO) for fruitful comments and valuable discussions. Michiel Slob (TU Delft), Ben Norder (TU Delft), Jacco Eversdijk (TNO) and Jelle Rohlfs (TNO) are greatly acknowledged for their technical support. We are thankful to Sian Jones (TU Delft) for proofreading the paper and to Stephen Eustace (TU Delft) and Guilhem Zwart for assistance with NMR analysis.

References

1 U. Eduok, R. Suleiman, M. Khaled and R. Akid, *Prog. Org. Coat.*, 2016, **93**, 97–108.
2 M. Fadil, D. S. Chauhan and M. A. Quraishi, *Russ. J. Appl. Chem.*, 2018, **91**, 1721–1728.
3 R. Suleiman, H. Dafalla and B. El Ali, *RSC Adv.*, 2015, **5**, 39155–39167.
4 A. A. Keller, H. Wang, D. Zhou, H. S. Lenihan, G. Cherr, B. J. Cardinale, R. Miller and Z. Ji, *Environ. Sci. Technol.*, 2010, **44**, 1962–1967.
5 N. Saleh, T. Phenrat, K. Sirk, B. Dufour, J. Ok, T. Sarbu, K. Matyjaszewski, R. D. Tilton and G. V. Lowry, *Nano Lett.*, 2005, **5**, 2489–2494.
6 V. K. Sharma, K. M. Siskova, R. Zboril and J. L. Gardea-Torresdey, *Adv. Colloid Interface Sci.*, 2014, **204**, 15–34.
7 S. Akbari, S. M. Mahmood, I. M. Tan, H. Ghaedi and O. L. Ling, *Polymers*, 2017, **9**(12), 647.
8 M. Algharaib, A. Alajmi and R. Gharbi, *J. Pet. Sci. Eng.*, 2014, **115**, 17–23.
9 T. Yuan, Z. Liu, R. Gao, G. Hu, G. Zhang and J. Zhao, *J. Appl. Polym. Sci.*, 2018, **135**, 46086.
10 J. E. O. Mayne, *J. Appl. Chem.*, 1959, **9**, 673–680.
11 R. J. L. W. Lake, W. Rossen and G. Pope, *Fundamentals of enhanced oil recovery*, Society of Petroleum Engineers, 2014.
12 K. S. Sorbie, *Polymer-Improved Oil Recovery*, Springer, Netherlands, 1991.
13 J. Sheng, *Modern Chemical Enhanced Oil Recovery: Theory and Practice*, Gulf Professional Publishing, 2010.
14 M. Mirzaie Yegane, E. Battistutta and P. Zitha, presented in part at the SPE Europec featured at 81st EAGE Conference and Exhibition, London, England, UK, 2019/6/3, 2019.
15 B. Al-Shakry, T. Skauge, B. Shaker Shiran and A. Skauge, *Energies*, 2019, **12**(1), 49.
16 G. Chauveteau, *Water-Soluble Polymers*, American Chemical Society, 1986, ch. 14, vol. 213, pp. 227–267.
17 S. Peng and C. Wu, *Macromolecules*, 1999, **32**, 585–589.
18 I. Ohmine and T. Tanaka, *J. Chem. Phys.*, 1982, **77**, 5725.
19 A. Moradi-Araghi and P. H. Doe, *SPE*, 1987, **2**(2), 189–198.
20 D. N. Schulz, J. J. Kaladas, J. J. Maurer, J. Bock, S. J. Pace and W. W. Schulz, *Polymer*, 1987, **28**, 2110–2115.
21 C. Senan, J. Meadows, P. T. Shone and P. A. Williams, *Langmuir*, 1994, **10**, 2471–2479.
22 A. Durand and D. Hourdet, *Polymer*, 1999, **40**, 4941–4951.
23 D. Levitt and G. A. Pope, presented in part at the SPE Symposium on Improved Oil Recovery, Tulsa, Oklahoma, USA, 2008/1/1, 2008.
24 P. H. Doe, A. Moradi-Araghi, J. E. Shaw and G. A. Stahl, *SPE Reservoir Eng.*, 1987, **2**, 461–467.

25 R. Klucker, F. Candau and F. Schosseler, *Macromolecules*, 1995, **28**, 6416–6422.
26 E. C. M. Vermolen, M. J. T. Van Haasterecht, S. K. Masalmeh, M. J. Faber, D. M. Boersma and M. A. Gruenenfelder, presented in part at the SPE Middle East Oil and Gas Show and Conference, Manama, Bahrain, 2011/1/1, 2011.
27 F. G. C. Tessarolli, S. T. S. Souza, A. S. Gomes and C. R. E. Mansur, *Gels*, 2019, **5**, 7.
28 L. Petit, L. Bouteiller, A. Brûlet, F. Lafuma and D. Hourdet, *Langmuir*, 2007, **23**, 147–158.
29 D. Portehault, L. Petit, N. Pantoustier, G. Ducouret, F. Lafuma and D. Hourdet, *Colloids Surf., A*, 2006, **278**, 26–32.
30 D. Hourdet and L. Petit, *Macromol. Symp.*, 2010, **291–292**, 144–158.
31 W.-C. Lin, W. Fan, A. Marcellan, D. Hourdet and C. Creton, *Macromolecules*, 2010, **43**, 2554–2563.
32 D. Portehault, L. Petit and D. Hourdet, *Soft Matter*, 2010, **6**, 2178–2186.
33 M. Kamibayashi, H. Ogura and Y. Otsubo, *Ind. Eng. Chem. Res.*, 2006, **45**, 6899–6905.
34 P. Bhardwaj, S. Singh, V. Singh, S. Aggarwal and U. K. Mandal, *Int. J. Polym. Mater. Polym. Biomater.*, 2008, **57**, 404–416.
35 A. Maghzi, R. Kharrat, A. Mohebbi and M. H. Ghazanfari, *Fuel*, 2014, **123**, 123–132.
36 Z. Hu, M. Haruna, H. Gao, E. Nourafkan and D. Wen, *Ind. Eng. Chem. Res.*, 2017, **56**, 3456–3463.
37 J. Cao, T. Song, Y. Zhu, X. Wang, S. Wang, J. Yu, Y. Ba and J. Zhang, *RSC Adv.*, 2018, **8**, 38056–38064.
38 D. Zhu, L. Wei, B. Wang and Y. Feng, *Energies*, 2014, **7**, 3858–3871.
39 P. Greenwood, *Pigm. Resin Technol.*, 2011, **40**, 275–284.
40 S. R. Saunders, M. R. Eden and C. B. Roberts, *J. Phys. Chem. C*, 2011, **115**, 4603–4610.
41 S. Skoglund, T. A. Lowe, J. Hedberg, E. Blomberg, I. O. Wallinder, S. Wold and M. Lundin, *Langmuir*, 2013, **29**, 8882–8891.
42 T. Phenrat, N. Saleh, K. Sirk, H.-J. Kim, R. D. Tilton and G. V. Lowry, *J. Nanopart. Res.*, 2008, **10**, 795–814.
43 X. Y. Wu, D. Hunkeler, A. E. Hamielec, R. H. Pelton and D. R. Woods, *J. Appl. Polym. Sci.*, 1991, **42**, 2081–2093.
44 I. Blute, R. J. Pugh, J. van de Pas and I. Callaghan, *J. Colloid Interface Sci.*, 2007, **313**, 645–655.
45 F. Book, M. T. Ekvall, M. Persson, S. Lönnerud, T. Lammel, J. Sturve and T. Backhaus, *NanoImpact*, 2019, **13**, 100–111.
46 R. Aveyard, B. P. Binks and J. H. Clint, *Adv. Colloid Interface Sci.*, 2003, **100–102**, 503–546.
47 D. N. Benoit, H. Zhu, M. H. Lilierose, R. A. Verm, N. Ali, A. N. Morrison, J. D. Fortner, C. Avendano and V. L. Colvin, *Anal. Chem.*, 2012, **84**, 9238–9245.
48 L. C. F. Andrade, J. A. Petronílio, C. E. de A. Maneschy and D. O. de A. Cruz, *J. Braz. Soc. Mech. Sci. Eng.*, 2007, **29**, 162–167.
49 E. M. Hotze, T. Phenrat and G. V. Lowry, *J. Environ. Qual.*, 2010, **39**, 1909–1924.
50 J. Israelachvili, *Intermolecular and Surface Forces*, Academic Press, 3rd edn, 2011.
51 S. R. Raghavan, J. Hou, G. L. Baker and S. A. Khan, *Langmuir*, 2000, **16**, 1066–1077.
52 H. Ohshima, *J. Colloid Interface Sci.*, 1995, **174**, 45–52.
53 T. Tadros, *General Principles of Colloid Stability and the Role of Surface Forces*, 2014, pp. 1–22, DOI: 10.1002/9783527631193.ch1.
54 B. Vincent, J. Edwards, S. Emmett and A. Jones, *Colloids Surf.*, 1986, **18**, 261–281.
55 A. Jones and B. Vincent, *Colloids Surf.*, 1989, **42**, 113–138.
56 M. Moskovits and B. Vlčková, *J. Phys. Chem. B*, 2005, **109**, 14755–14758.
57 J. C. Berg, *An Introduction to Interfaces & Colloids, The Bridge to Nanoscience*, World Scientific Publishing Co. Pte. Ltd, Singapore, 2010.
58 C. O. Metin, R. T. Bonnecaze, L. W. Lake, C. R. Miranda and Q. P. Nguyen, *Appl. Nanosci.*, 2014, **4**, 169–178.
59 C. Omurlu, L. Lake, C. Miranda and Q. P. Nguyen, *J. Nanopart. Res.*, 2011, **13**, 839–850.
60 A. J. Worthen, V. Tran, K. A. Cornell, T. M. Truskett and K. P. Johnston, *Soft Matter*, 2016, **12**, 2025–2039.
61 C. A. Silvera Batista, R. G. Larson and N. A. Kotov, *Science*, 2015, **350**(6257), 1242477.
62 A.-R. Mahdavian, M. Abdollahi and H. R. Bijanzadeh, *J. Appl. Polym. Sci.*, 2004, **93**, 2007–2013.
63 B. Al-Shammari, T. Al-Fariss, F. Al-Sewailm and R. Elleithy, *J. King Saud Univ., Eng. Sci.*, 2011, **23**, 9–14.
64 A. Ait-Kadi, P. J. Carreau and G. Chauveteau, *J. Rheol.*, 1987, **31**, 537.
65 S. Berg and J. van Wunnik, *Transp. Porous Media*, 2017, **117**, 229–246.

